Hydrothermal preparation and photocatalytic properties of $Y_2Sn_2O_7$ nanocrystals

KunWei Li, Hao Wang*, Hui Yan

The College of Materials Science and Engineering, Beijing University of Technology, Beijing 100022, China

Abstract

Nanosized $Y_2Sn_2O_7$ powder photocatalysts with different particle sizes were synthesized through the low temperature hydrothermal method by using different organic agents. The samples were characterized by X-ray diffractometer (XRD), scanning electron microscope (SEM), transmission electron microscope (TEM), surface area and porosity analyzer, and ultraviolet–visible (UV–vis) spectroscopes. Photocatalytic measurements showed $Y_2Sn_2O_7$ nanocrystals with about 10 nm particle sizes possess superior photocatalytic properties in water purification and may find potential application in related fields.

1. Introduction

Rare earth pyrochlore $Y_2Sn_2O_7$ is of considerable importance for numerous applications including piezoelectricity, dielectric, resistance to radiation damage, and have been specially investigated as heterogeneous catalysts for a variety of processes [1–4]. The extensive application of these complex oxides may be partially understood as being related to the stability of pyrochlore and the morphologies and sizes of particles which in turn largely depend on the preparation methods and preparation conditions. In general, phase pure, nanosized $Y_2Sn_2O_7$ with a narrow size distribution is highly desirable to serve most of their intended purposes, especially in the catalysts and rapidly developing nanoelectronic and nanooptoelectronic devices.

Great efforts have been made to devise versatile techniques such as high temperature solid state reaction [5], co-precipitation [6], sol–gel [7] and so forth, to synthesize pyrochlore $Y_2Sn_2O_7$. The above conventional methods for the preparation of complex pyrochlore oxides are troublesome as they all employ a relatively high temperature (ca. 1000 °C) for a very long time. Moreover, as well known, the high temperature solid state reaction method can easily lead to local chemical heterogeneity and large sized particles, which may result in multiphase powders [8]. On the other hand, soft chemical methods have offered an alternative to produce smaller sized, chemically homogeneous particles [9]. The use of solution-based soft chemical methods to prepare nanocrystalline materials is expected to result in chemically homogeneous and phase-pure specimens, a narrow particles size distribution, and low crystallization temperatures of the materials. However, as far as we know, there have been only a few previous studies [10] on the hydrothermal synthesis of rare earth stannates and there is no study on the particle sizes control of rare earth stannates with pyrochlore structure.

In this work, soft chemical method was introduced to synthesize and control the particle sizes of yttrium tin ($Y_2Sn_2O_7$) pyrochlore by using different organic agents through low temperature (180 °C) hydrothermal technique. The products showed nanosphere morphology and possessed superior photocatalytic properties in water purification and may find potential application in related fields.

2. Experiments

2.1. Samples preparation

The starting reagents were analytical grade yttrium nitrate hydrate, $Y(NO_3)_3 \cdot 6H_2O$ and tin chloride hydrate, $SnCl_4 \cdot 5H_2O$. The exact quantity of Y and Sn in the nitrate hydrate and chlo-

* Corresponding author. Tel.: +86 10 67392733; fax: +86 10 67392412.
  E-mail address: haowang@bjut.edu.cn (H. Wang).

ride hydrate was determined by thermo gravimetric analysis. An amount of $Y(NO_3)_3 \cdot 6H_2O$ and $SnCl_4 \cdot 5H_2O$ were dissolved in deionized water, respectively. And then, an amount of organic agent (polymethyl methacrylate: PMMA, cetyltrimethyl ammonium bromide: CTAB or ethylene diamine tetraacetic acid: EDTA) and the equal molar ratios of $SnCl_4$ solution were, respectively, added in the $Y(NO_3)_3$ solution while stirring vigorously on a magnetic stirrer. Then some amount of NaOH solution was dropped to the above solution to form white precipitation mixtures with different nominal NaOH concentrations. The mixture was stirred at ambient temperature for 10 min and then sealed in a 50-ml stainless autoclave Teflon lined and allowed to heat at 180 °C for 12 h under autogenous pressure. After natural cooling, the products were filtered off, washed with deionized water, and dried at 110 °C.

2.2. Characterization of the samples

The X-ray diffraction (XRD) analysis was performed in θ–2θ mode using a Bruker D8 X-ray diffractometer with a focusing Ge (1 1 1) incident beam monochromator (Cu $K\alpha_1$ radiation, $\lambda = 1.5406$ Å). Scanning electron microscopy (SEM) images of samples were obtained with a Hitachi model S-3500N scanning electron microscope. Transmission electron microscopy (TEM), selected area electron diffraction (SAED) and high resolution transmission electron microscopy (HRTEM) images were taken on a JEOL-JEM 2010F transmission electron microscope, using an accelerating voltage of 200 kV. The surface areas of the powders were determined by a Micromeritics ASAP 2020 surface area and porosity analyzer in the method of Brunauer–Emmett–Teller (BET) nitrogen adsorption and desorption. Optical absorption studies were carried out using a UV–vis–NIR spectrophotometer (Shimadzu UV-3101PC).

The photocatalytic property of the products was tested in our house-made instruments. At first, 0.2 g product was dispersed into five beakers which were filled with 100 ml 10 mg/l methyl orange solution separately, and be irritated under ultraviolet light by using a light resource (400 W high-pressure Hg lamp) for different time, then be characterized by UV–vis spectroscopy.

3. Results and discussion

In order to get the suitable temperature and NaOH concentrations, samples were synthesized under different NaOH concentrations (a: 0 M; b: 1 M; c: 3 M) at 180 °C for 12 h. As can be seen from the XRD patterns in Fig. 1, three kinds of materials were formed at different NaOH concentrations. Fig. 1a was ascribed to cassiterite SnO_2 with tetragonal system (JCPDS 411445), while Fig. 1c was attributed to yttrium hydroxide $Y(OH)_3$ with the hexagonal system (JCPDS 832042). All diffraction lines in Fig. 1b can be readily indexed to a pure cubic phase $Y_2Sn_2O_7$ with pyrochlore structure conforming to the $Fd3m$ space group (JCPDS 201418). It could be seen that the concentration of NaOH played a critical role in the formation of phase-pure yttrium tin pyrochlore ($Y_2Sn_2O_7$) by hydrothermal method.
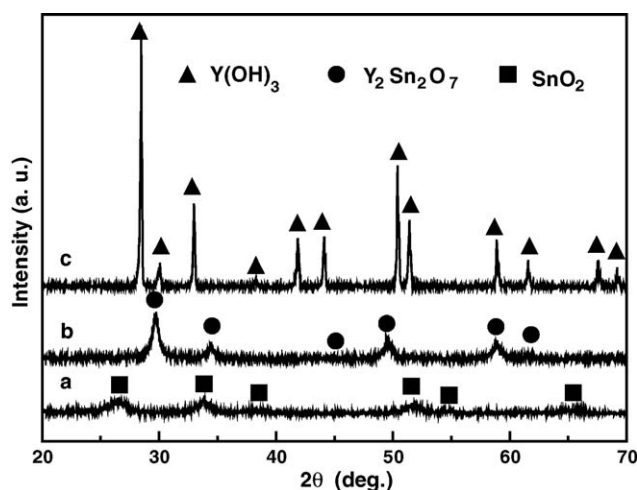

Fig. 1. XRD patterns of the samples synthesized under different NaOH concentrations (a: 0 M; b: 1 M; c: 3 M) by hydrothermal method at 180 °C for 12 h.

Fig. 2 shows the XRD patterns of the samples synthesized, respectively, without any organic agent: a; with PMMA: b; with CTAB: c; with EDTA: d; sample a was annealed at 1000 °C for 2 h: e. From Fig. 2, all diffraction lines in the patterns can be readily indexed to a pure cubic phase $Y_2Sn_2O_7$ with pyrochlore structure conforming to the $Fd3m$ space group (JCPDS 201418). We can see that the FWHM values of the main peaks decrease from sample a to sample e. According to the Scherrer formula, the crystallite size is in inverse proportion to the FWHM values of the main peaks. Therefore, the average particle sizes of the samples gradually become large from sample a to sample e.

Fig. 3 shows the TEM micrograph of the samples a–c and SEM micrograph of samples d and e. The inserted pattern in Fig. 3c was the SAED of the sample c; Fig. 3f was the HRTEM image of the sample c. As can be seen from Fig. 3a and b, the particles with an average diameter of about 10 nm had been obtained. SEM observation revealed that the synthesized rare earth stannates have a relatively narrow size distribution and uni-
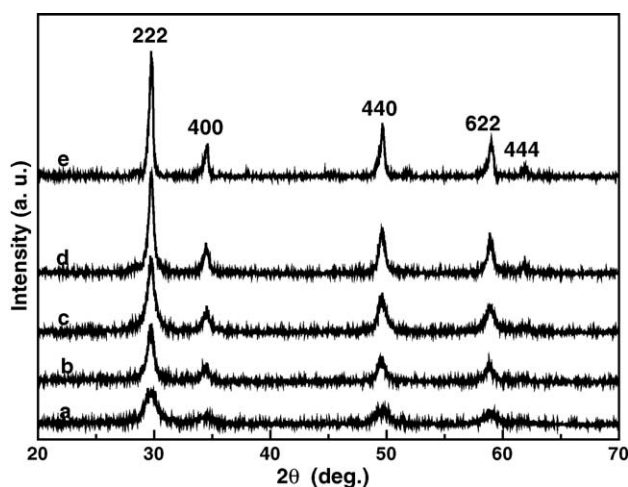

Fig. 2. XRD patterns of the samples synthesized, respectively, without any organic agent: a; with PMMA: b; with CTAB: c; with EDTA: d; sample a was annealed at 1000 °C for 2 h: e (the samples a–e in Figs. 3–6 have the same meanings as those in this figure).
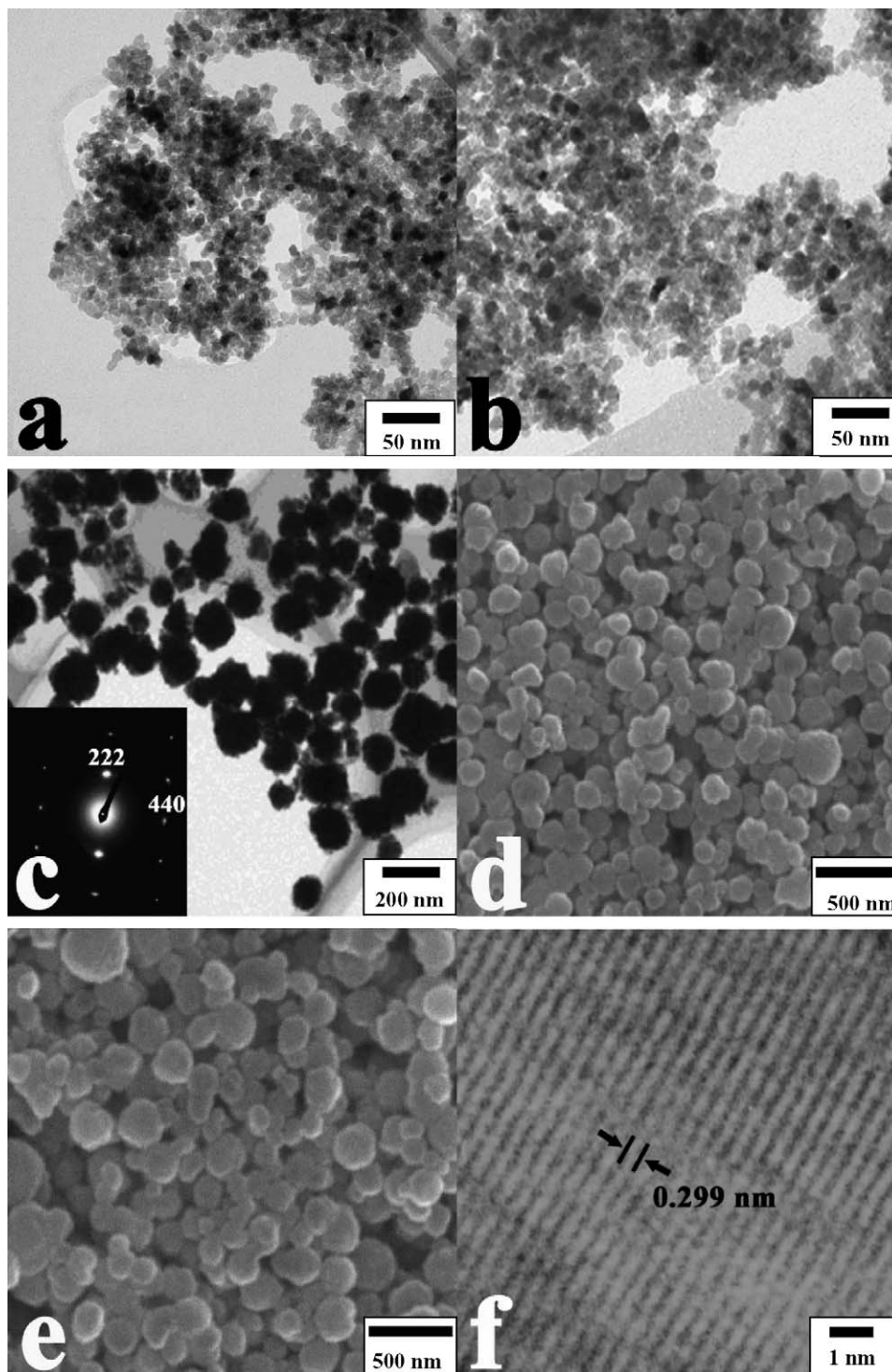
Fig. 3. TEM micrograph of the samples a–c and SEM micrograph of samples d and e. The inserted pattern in subpart 'c' was the SAED of the sample c; subpart 'f' was the HRTEM image of the sample c.

form shape with a rough surface structure. The average particle sizes of the samples c–e were about 100, 200 and 300 nm, respectively. The highly arrayed diffraction spots in Fig. 3c inserted image indicate the single-crystalline property of the $Y_2Sn_2O_7$ nanosphere. Fig. 3f shows the HRTEM image recorded from the $Y_2Sn_2O_7$ nanosphere shown in Fig. 3c. The regular spacing of the observed lattice planes was about 0.299 nm, which is con-

sistent with the (2 2 2) lattice spacing of $Y_2Sn_2O_7$, showing that the nanosphere was of uniform crystal structure.

Based on the above experiments and results, we suggest the formation mechanism of the $Y_2Sn_2O_7$ nanoparticles with different sizes in the presence of organic agents as follows.

In these experiments, the functions of organic agents with Y^{3+} rest with three kinds of different mechanisms. EDTA is a

strong complex reagent with Y^{3+} ($K_{EDTA-Y^{3+}} = 10^{17.38}$) [11], which leads to the formation of the stable Y–EDTA complexes. CTAB is a surfactant with a surface active cation, which can not complex with Y^{3+}. However, in the alkaline solution, due to the hydrolyzation of yttrium ions, yttrium ions exists in the forms of polyhydroxylated compound with negative electric charges which may react with the surface-active cation of CTAB to form ion pairs [12]. PMMA is an organic high molecular compound with no electric charge, which does not react with Y^{3+} in the solution. However, the existence of PMMA may increase the viscosity of solution and then decrease the diffusion coefficient of Y^{3+} under the reaction condition.

Usually, the productions of $Y_2Sn_2O_7$ nanocrystals include two main processes, the formation of nucleus and the growth of crystal. The less number of the nucleus will lead to the larger particle size at the constant initial concentration of source ions. In the initial stage of the experiment, clusters with critical size would be formed, which could act as nucleus for $Y_2Sn_2O_7$ crystals and develop into crystallite under the hydrothermal conditions. The number of these clusters is determined by the initial concentration of free Y^{3+} ions which will be controlled by the stability of Y–EDTA complex, Y–CTAB ion pair, and be affected by the viscosity of the solution. The formation of the Y–EDTA complex sharply decreased the free Y^{3+} concentration in the solution, and effectively prevented the formation of the clusters in the presence of EDTA [13]. Therefore, the particle sizes of the samples are relatively larger than the others. The formation of Y–CTAB ion pair in the alkaline solution decreased the free Y^{3+} concentration to some extent. Therefore, the particle sizes of the samples are relative smaller than the EDTA samples. When there were not any organic agents in the solution, the higher free Y^{3+} concentration led to the formation of larger number of the clusters, and then the particle sizes decreased. The experiment verified that the extent of effect of PMMA on the particle sizes under the hydrothermal condition is not obvious. This may result from the decrease of the solution viscosity under the hydrothermal condition [14].
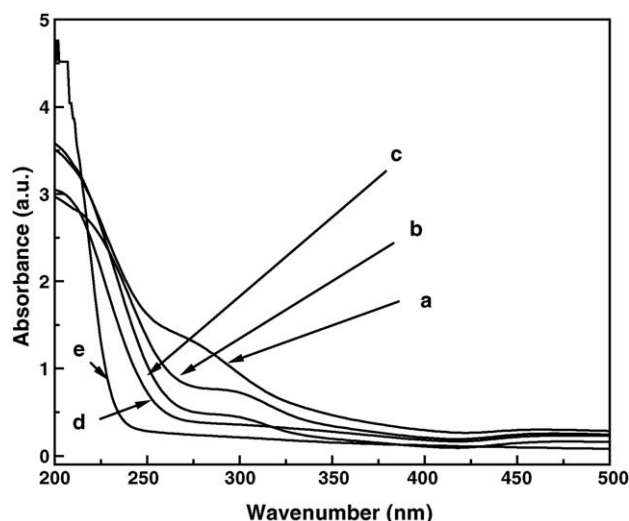
Fig. 4 shows the whole UV–vis spectra of the as-synthesized $Y_2Sn_2O_7$ samples. As can be seen from the figure, the absorbance edges of $Y_2Sn_2O_7$ samples a–e varied regularly. With the decrease of sample particle size, the absorbance edges of samples move to long wavelength, that is to say, the red shift occurs. The absorbance edge of $Y_2Sn_2O_7$ sample a, with about 10 nm particle size, is approximate to that of TiO_2 [15,16]. As well known, the blue shift phenomenon mainly resulted from quantum size effect widely occurs in the absorption of nanoparticle size [17]. At the same time, due to the decrease of the particle size, the particle internal stress will increase, which will lead to the change of the energy gap structure [18], and the increase of electron wave function overlap [19], and the narrowing of the energy gap, and the red shift of absorption edges. In this experiment, the effect of quantum size effect may be less than that of the particle internal stress. Therefore, red shift occurred. These red shift phenomena in respect to the absorption onset had also been observed in II–VI semiconductor nanocrystals [20,21].

The surface areas of samples are summarized in Table 1. The surface area of the sample a was approximately 102 m^2/g. With the addition of the CTAB and EDTA, the surface areas reduced to 63 and 30 m^2/g, respectively. However, the addition of the PMMA did not obviously reduce the surface areas of the sample b. It indicates that different kinds of organic agents result in the difference in the particle sizes, and the surface areas of the samples. At the same time, the surface areas varied with the heat treatment temperature. When the sample was annealed at 1000 °C for 2 h, the surface areas were significantly reduced from 102 to 4.3 m^2/g.

Fig. 5 gives the depigmentation curves of methyl orange solutions with the addition of $Y_2Sn_2O_7$ sample a under ultraviolet light. Curve 'a' shows the depigmentation curve of absolute methyl orange solution without any $Y_2Sn_2O_7$ sample a irritated under ultraviolet light for 50 min, while other curves denote methyl orange solution with 2 g/l $Y_2Sn_2O_7$ samples a irritated under ultraviolet light for different time (b: 10 min; c: 20 min; d: 30 min; e: 40 min; f: 50 min). Seen from the pattern, the solutions with $Y_2Sn_2O_7$ sample a depigmented gradually and were almost decolored totally when the irritated time was up to 50 min. Obviously, $Y_2Sn_2O_7$ sample a played the role of photocatalyst.

Fig. 6 shows methyl orange solution decomposition ratio with the role of above five samples and Degussa P-25 (TiO_2) under ultraviolet light for different time. Seen from the results, the solutions depigmented gradually with enlonged irritation time. After 50 min, the decomposition ratio of methyl orange solution with $Y_2Sn_2O_7$ sample a reached to 95% while is still lower than

Fig. 4. The whole UV–vis spectra of the as-synthesized $Y_2Sn_2O_7$ samples.

Table 1
BET surface areas of the samples a–e synthesized with different organic agents

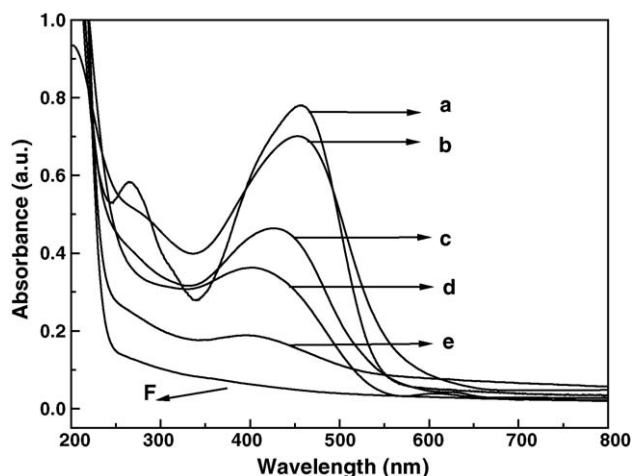| Samples	The synthetic condition	BET surface area (m^2/g)
a	Without any organic agent	102.5354
b	PMMA	100.6588
c	CTAB	63.0372
d	EDTA	30.1467
e	Sample a was annealed at 1000 °C for 2 h	4.3117

Fig. 5. The depigmentation curves of methyl orange solutions with the addition of $Y_2Sn_2O_7$ sample a under ultraviolet light.

the solution with TiO_2 whose rate is up to nearly 100%. In spite of this, $Y_2Sn_2O_7$ sample a may find potentially application due to its chemical and structural stability in solution. Comparatively, the photocatalytic abilities of other $Y_2Sn_2O_7$ samples are weaker than sample a, its decomposition ratio is just 80, 70, 45 and 16% after 50 min, respectively. It may be resulted from the reduction of the sample surface area leading to the decrease of the active sites on the surface of samples.

The mechanism for photocatalytic degradation of organic pollution on the solid catalysis always depicted as follows: a continuous band-gap irradiation of aqueous semiconductor dispersion excites an electron from the valence band to the conduction band, creating an electron–hole pair. The photogenerated holes are considered capable of directly oxidizing many organic compounds. However, the recombination of the electron–hole pairs will decrease the photocatalytic activity. At first, in our experiments, when the particle size is smaller than 10 nm, the photogenerated carrier diffuse quickly from center to the surface [22], leading to the higher separation efficiency
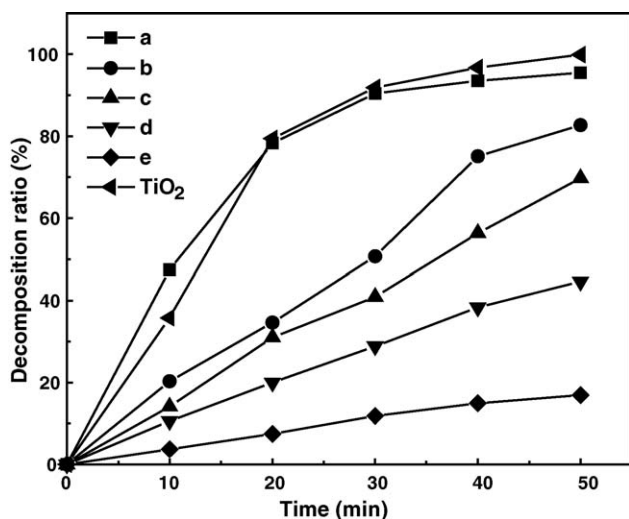
photogenerated electron–hole pairs and the higher photocatalytic activity of particles. Secondly, due to the energy gap becoming relatively small with the decrease of particle size, the number of photogenerated electron–hole pairs increased, resulting in the increasing of photocatalytic ability. Thirdly, the increasing of specific surface area leads to the increasing of absorption ability to organics, and then heightens the photocatalytic degradation ability to organics. In the end, the higher photocatalytic activity of $Y_2Sn_2O_7$ against methyl orange should have some connection with the SnO_6 octahedrons in the crystalline structures. A study on luminescent properties of tantalates and niobates has shown that the closer the bond angle of M−O−M is to180 °C, the more the excitation energies delocalized [23,24]. This means that the bond angle of M−O−M in MO_6 octahedrons is one of the important factors affecting the photocatalytic and photophysical properties of semiconductors. The bond angle of Sn−O−Sn in $Y_2Sn_2O_7$ is close to ideal 180 °C, so it might facilitate the movement of photogenerated electron–hole pairs and eliminate the re-combination of electron–hole pairs and finally increase the catalytic activity of methyl orange decomposition.

4. Conclusions

In summary, the nanosized $Y_2Sn_2O_7$ with the particle size from 10 to 300 nm have been synthesized through the low temperature hydrothermal method with the presences of different organic agents. The red shift phenomena depended on nanoparticle size were observed in the UV–vis spectra of the as-synthesized $Y_2Sn_2O_7$ samples. Photocatalytic measurements through the photo-depigmentation of methyl orange showed $Y_2Sn_2O_7$ nanocrystals with about 10 nm particle sizes possess superior photocatalytic properties in water purification and may find potential application in related fields. At the other hand, the synthesis method adopted in this paper may be applied in the synthesis of other pyrochlore compounds.

References

[1] C.G. Whinfrey, D.W. Eckart, A. Tauber, J. Am. Chem. Soc. 82 (1960) 2695.
[2] M.A. Subramania, G. Aravamudam, G.V. Subba Rao, Prog. Solid State Chem. 15 (1983) 55.
[3] S. Ishida, F. Ren, N. Takeuchi, J. Am. Ceram. Soc. 10 (1993) 2644.
[4] J.H. Zhao, H.P. Kunkel, M.A. Subramanian, Phys. Rev. Lett. 83 (1999) 219.
[5] Ismunandar, B.J. Kennedy, B.A. Hunter, T. Vogt, J. Solid State Chem. 131 (1997) 317–325.
[6] V. Ravi, S. Adyanthaya, M. Aslam, S. Pethkar, V.D. Choube, Mater. Lett. 40 (1999) 11–13.
[7] Z.G. Lu, J.W. Wang, Y.G. Tang, Y.D. Li, J. Solid State Chem. 177 (2004) 3075.
[8] M.A. Subramanian, G. Aravamudan, G.V. Subba Rao, Prog. Solid State Chem. 15 (1983) 55.
[9] S.M. Zanetti, S.A. da Silva, G.P. Thim, J. Solid State Chem. 177 (2004) 4546.
[10] J. Moon, M. Awano, K. Maeda, J. Am. Ceram. Soc. 84 (2001) 2531.
[11] Y.G. Wang, Y. Xiong, S.L. Meng, D.Q. Li, Talanta 63 (2004) 239.

Fig. 6. The decomposition ratio of methyl orange solution with the role of $Y_2Sn_2O_7$ samples and TiO_2 under ultraviolet light for different time.

[12] Q.S. Huo, D.I. Margolese, U. Ciesla, D.G. Demuth, P.Y. Feng, T.E. Gier, P. Sieger, A. Firouzi, B.F. Chmelka, F. Schuth, G.D. Stucky, Chem. Mater. 6 (1994) 1176.

[13] R.E. Riman, W.L. Suchanek, K. Byrappa, C.W. Chen, P. Shuk, C.S. Oakes, Solid State Ionics 151 (2002) 393.

[14] M. Yoshimura, J. Mater. Res. 13 (1998) 1091.

[15] Y. Kim II, S. Atherton, E.S. Brigham, T.E. Mallouk, J. Phys. Chem. 97 (1993) 11802.

[16] S.-K. Lee, P.K.J. Robertson, A. Mills, D. McStay, N. Elliott, D. McPhail, Appl. Catal. B: Environ. 44 (2003) 173.

[17] P. Ball, L. Garwin, Nature 355 (1992) 761.

[18] H. Fu, A. Zunger, Phys. Rev. B 56 (1997) 1496.

[19] C.A. Smith, H.W.H. Lee, V.J. Leppert, S.H. Risbud, Appl. Phys. Lett. 75 (1999) 1688.

[20] A.L. Rogach, A. Kornowski, M. Gao, A. Eychmuller, J. Phys. Chem. B 103 (1999) 3065.

[21] H.J. Chang, C.Z. Lu, Y. Wang, C.S. Son, S. Kim, Y. Kim, I. Choi, J. Korean Phys. Soc. 45 (2004) 959.

[22] G. Rothenberger, J. Moser, M. Graetzel, N. Serpone, D.K. Sharma, J. Am. Chem. Soc. 107 (1985) 8054.

[23] G. Blasse, J. Solid State Chem. 72 (1988) 72.

[24] A.M. Srivastsva, J.F. Ackerman, J. Solid State Chem. 134 (1977) 187.